Transonic aeroelastic numerical simulation in aeronautical engineering

Guowei Yang [a]

[a] LHD of the Institute of Mechanics, Chinese Academy of Sciences, Beijing, P. R. China

PLEASE SCROLL DOWN FOR ARTICLE

Taylor & Francis
Taylor & Francis Group

Transonic aeroelastic numerical simulation in aeronautical engineering

GUOWEI YANG*

LHD of the Institute of Mechanics, Chinese Academy of Sciences, Beijing, 100080, P. R. China

A lower–upper symmetric Gauss–Seidel (LU-SGS) subiteration scheme is constructed for time-marching of the fluid equations. The Harten–Lax–van Leer–Einfeldt–Wada (HLLEW) scheme is used for the spatial discretization. The same subiteration formulation is applied directly to the structural equations of motion in generalized coordinates. Through subiteration between the fluid and structural equations, a fully implicit aeroelastic solver is obtained for the numerical simulation of fluid/structure interaction. To improve the ability for application to complex configurations, a multiblock grid is used for the flow field calculation and transfinite interpolation (TFI) is employed for the adaptive moving grid deformation. The infinite plate spline (IPS) and the principal of virtual work are utilized for the data transformation between the fluid and structure. The developed code was first validated through the comparison of experimental and computational results for the AGARD 445.6 standard aeroelastic wing. Then, the flutter character of a tail wing with control surface was analyzed. Finally, flutter boundaries of a complex aircraft configuration were predicted.

Keywords: Aeronautical engineering; Fluid structure; Aeroelasticity; Flutter

1. Introduction

Until the last decade, aeroelastic analyses mainly used linear methods to calculate the unsteady fluid loads and to solve the structural equation of motion. When structural deformation becomes large, the structural nonlinear character needs to be considered. However, for the flutter analyses of vehicle design, only the flutter boundaries are concerned, the linear assumption for the structural deformation is reasonable. Under the conditions of low Mach number and small angle of attack, aerodynamic loads can be obtained by the linear theory. For the transonic flow, in the presence of a strong shock wave and shock induced flow separation, only the unsteady Euler and Navier–Stokes fluid governing equations can predict the aerodynamic loads correctly. In the last decade, with the development of computational methods, numerical analyses of nonlinear transonic fluid/structure interaction have become reality (Lee-Rausch and Batina 1996, Gordnier and Melville 2000, Yang *et al.* 2003 and Guruswamy 1990). Since the flutter analyses concern mainly the fluid/structural interaction at small angles of attack, in order to improve the computational efficiency, the inviscid Euler equations were chosen as the fluid governing equations for the many of flutter computations (Goura *et al.* 2001a and Liu *et al.* 2001).

For steady flow simulation, due to only the solution of time independence concerned, many higher accuracy schemes of spatial discretization were developed. The implicit time-marching scheme was developed for the increase of time-step size and the improvement of computational efficiency. Therefore, most of the implicit time-marching schemes have only first order accuracy. For unsteady flutter calculations, the computational time-accuracy is of the same importance as the spatial discretization accuracy. Even the use of a higher order accurate scheme for the time-marching, if the flow governing equations are only loosely coupled with structural equations of motion, namely, after the aerodynamic loads are determined by solving the flow governing equations, the structural model is used to update the position of body. The coupling contains the error of one time step, thus the whole calculations are always only

* Email: gwyang@imech.ac.cn

first-order accurate in time regardless of the temporal accuracy of the individual solvers of the flow and structural equations. The loosely coupled methods were used for most of the present flutter simulations.

A fully implicit aeroelastic approach was first put forward by Alonso and Jameson (1994) for 2D Euler aeroelastic simulation, called the dual-time implicit–explicit method. In each real time step, the time-accurate solution is solved by explicit Runge–Kutta time-marching method for a steady problem, so all convergence acceleration techniques such as multigrid, residual averaging and local time-step can be implemented in the calculation. In general, about 100 pseudo-time steps are needed for the explicit iterations to ensure adequate convergence, thus the method is still very time-consuming, so far as the authors know only 3D Euler results were reported (Liu *et al.* 2001). Based on the same thought, Goura *et al.* (2001a) constructed a first-order implicit time-marching scheme as well as only first-order spatial discretization in the implicit side for the solution of a pseudo steady flow. The second-order temporal and spatial accuracy is obtained at pseudo steady flow convergence. Melville *et al.* (1997) proposed a fully implicit aeroelastic solver between the fluids and structures, in which a second-order approximate factorization scheme with subiterations was performed for the flow governing equations and the structural equations were cast in an iterative form. Since the restricted number of iterations cannot remove sequencing effects and factorization errors completely at every time step, a relatively small time step was used in their calculation. Nevertheless, a fully implicit aeroelastic Navier–Stokes solver with three subiterations has succeeded in the flutter simulation for an aeroelastic wing (Gordnier and Melville 2000). The authors constructed a subiteration scheme based on lower–upper symmetric Gauss–Seidel (LU-SGS) scheme, a fully implicit multi-block solver was developed for the predictions of flutter boundaries and aileron buzz for a supersonic transport model (Yang *et al.* 2003).

In the flutter calculation, due to the deformation of the aeroelastic configuration, adaptive dynamic grids need to be generated at each time step. At present, many aeroelastic calculations are only done for an isolated wing with single-block grid topology. For the simple flexible geometry, the grid can be completely regenerated with an algebraic method or a simple grid deformation approach. For the complicated aerodynamic configurations, multiblock grids are usually generated with elaborate elliptical method for steady flow simulation. However, for aeroelastic application, it is impossible to regenerate multiblock grids with the elaborate method at each time step due to the limitation of computational cost. Multiblock grid deformation approach needs to be used. Wong *et al.* (2000) established a multiblock moving mesh algorithm. The spring network approach is utilized only to determine the motion of the corner points of the blocks and the transfinite interpolation (TFI) method is applied to the edge, surface and volume grid deformations. Potsdam and Guruswamy (2001) also put forward a multiblock moving grid approach, which uses a blending method of a surface spline approximation and nearest surface point movement for block boundaries and TFI for the volume grid deformation.

Structural models may be given by a plate model, but the flow calculations are carried out for the full geometry. The interpolation between fluid and structure grids is required. Infinite and finite surface splines (Harder and Desmarais 1972 and Appa 1989) developed for the plate aerodynamics and plate structural model are still main interpolation tools, only the aerodynamic grid needs to be projected on the surface of the structural grid before interpolation. Goura *et al.* (2001b) suggested an interpolation method of constant volume transformation (CVT) for the data exchange between fluids and structures based on the local grid information.

In this paper, a fully implicit multiblock Navier–Stokes aeroelastic solver implemented by the authors was used for predictions of flutter phenomena on more complex configurations. One is the tail wing with control surface and another is a wing/body/tail aircraft model. The purpose of this work is to study the ability of the developed code for complex engineering problems. The comparison between calculation and experiment for the AGARD 445.6 standard aeroelastic wing (Yates 1988) is also shown in this paper.

2. Structural equation of motion

The second-order linear structural dynamic governing equation of motion can be written as

$$[M]\{\ddot{d}(t)\} + [C]\{\dot{d}(t)\} + [K]\{d(t)\} = \{F(t)\} \qquad (1)$$

where $[M]$, $[C]$, $[K]$ are mass, damping and stiffness matrices, respectively. Here, $\{d(t)\}$ is a displacement vector, and $\{F(t)\}$ is the aerodynamic load, which represents the coupling of the unsteady aerodynamic and inertial loads with the structural dynamics. This allows great flexibility in the choice of methods that can be used to model the system. For example, for linear structural models, the mass, damping and stiffness are constant with time or structure, which remains true independent of the aerodynamics. If the aerodynamic methods are linear, the structural equation of motion reduces to computation of the complex eigenvalues of the stability matrix in the frequency domain, whose values determine the stability of the system. If aerodynamics and/or structures are nonlinear, computations can only be performed in the time domain, which tends to complicate the process of determining system stability. In this paper, aerodynamic loads are solved by the nonlinear Navier–Stokes equations and the structural deformation is based on the linear assumption.

In order to solve equation (1), the Rayleigh–Ritz method is used. For a specific aerodynamic configuration, the natural mode shapes and frequencies can be calculated by the finite-element analysis or obtained from experimental influence coefficient measurements. In this study, the data of natural mode shapes and frequencies are

calculated by finite-element analysis. In general, only the first N modes are considered. With these first N modes, we have an approximate description of the displacement vector of the system given by

$$\{d(t)\} = [\Phi]\{q(t)\}. \tag{2}$$

Since the natural modes are orthogonal with respect to both the mass and stiffness matrices, premultiplying equation (1) by $[\Phi]^{\mathrm{T}}$ yields structural equations in generalized coordinates

$$\ddot{q}_i(t) + 2\zeta_i\omega_i\dot{q}_i(t) + \omega_i^2 q_i(t) = \frac{q_\infty \oint_S \int [\Phi]_i^{\mathrm{T}}\Delta Cp_i \, \mathrm{d}S}{M_i} \tag{3}$$

where

$$\omega_i^2 = [\Phi]_i^{\mathrm{T}}\{K\}[\Phi], \quad M_i = [\Phi]_i^{\mathrm{T}}\{M\}[\Phi],$$

$$\mathrm{d}_i(t) = \sum_{i=1}^{N} q_i(t)[\Phi]. \tag{4}$$

The equation (3) can be written as a first-order system by defining $\vec{S} = [q, \dot{q}]$

$$\dot{\vec{S}} = \vec{P} = -\begin{bmatrix} 0 & -1 \\ \omega_i^2 & 2\omega_i\zeta_i \end{bmatrix}\vec{S} + \begin{bmatrix} 0 \\ \frac{q_\infty \oint_S \int [\Phi]_i^{\mathrm{T}}\Delta Cp_i \, \mathrm{d}S}{M_i} \end{bmatrix}. \tag{5}$$

The equation can be discretized by a second-order scheme with subiteration based on Melville *et al.* (1997) as

$$\begin{bmatrix} 1 & -\phi^i\Delta\tau \\ \phi^i\Delta\tau\omega_i^2 & 1 + 2\phi^i\omega_i\zeta_i\Delta\tau \end{bmatrix}\Delta\vec{S}$$

$$= -\phi^i\left\{(1+\phi)\vec{S}^p - (1+2\phi)\vec{S}^n + \phi\vec{S}^{n-1} + \Delta\tau\vec{P}\right\} \tag{6}$$

where $\Delta\vec{S} = \vec{S}^{(p+1)} - \vec{S}^{(p)}$, $\phi^i = 1/(1 + \phi)$.

When $\phi = 0.5$ and $p \rightarrow \infty$, equation (6) has second order time accuracy.

3. Aerodynamic equations

Aerodynamic governing equations are the unsteady, 3D thin layer Navier–Stokes equations in strong conservation law form, which can be written in curvilinear space ξ, η, ζ and τ in non-dimensional form as

$$\partial_\tau\hat{Q} + \partial_\xi F + \partial_\eta G + \partial_\zeta H = Re^{-1}\partial_\zeta H_{\mathrm{v}} + S_{\mathrm{GCL}}. \tag{7}$$

In the formulation, the viscosity coefficient μ in H_{v} is computed as the sum of laminar and turbulent viscosity coefficients, which are evaluated by the Sutherland's law and Baldwin–Lomax model with the Degani–Schiff modification. Viscous term H_{v} is discretized by the second order central scheme and inviscid terms F, G, H are

discretized by the HLLE scheme (Einfeldt *et al.* 1991) and higher order interpolation of the primitive variables for the left and right states at the cell interface (Anderson *et al.* 1985) is used. The source term S_{GCL} in equation (1) is obtained from the geometric conservation law (Thomas and Lombard 1979) for moving mesh, which is defined as

$$S_{\mathrm{GCL}} = Q\lfloor\partial_t J^{-1} + \left(\frac{\xi_t}{J}\right)_\xi + \left(\frac{\eta_t}{J}\right)_\eta + \left(\frac{\zeta_t}{J}\right)_\zeta\rfloor. \tag{8}$$

LU-SGS method (Yoon and Jameson 1988) is reconstructed containing subiteration as the time-marching scheme. Second-order temporal accuracy is obtained by utilizing three-point backward difference in the subiteration procedure. The numerical algorithm can be deduced as

$$LD^{-1}U\Delta Q = -\phi^i\{(1+\phi)Q^p - (1+2\phi)Q^n$$

$$+ \phi Q^{n-1} - J\Delta\tau Q^p S_{\mathrm{GCL}}{}^p \tag{9}$$

$$+ J\Delta\tau\left(\delta_\xi F^p + \delta_\eta G^p + \delta_\zeta(H^p - H_{\mathrm{v}}^p)\right)\}$$

where

$$L = \bar{\rho}I + \phi^i J\Delta\tau\left(A_{i-1,j,k}^+ + B_{i,j-1,k}^+ + C_{i,j,k-1}^+\right),$$

$$D = \bar{\rho}I$$

$$U = \bar{\rho}I - \phi^i J\Delta\tau\left(A_{i+1,j,k}^- + B_{i,j+1,k}^- + C_{i,j,k+1}^-\right)$$

and

$$\bar{\rho} = 1 + \phi^i J\Delta\tau(\bar{\rho}(A) + \bar{\rho}(B) + \bar{\rho}(C)), \quad \phi^i = \frac{1}{(1+\phi)},$$

$$\Delta Q = Q^{p+1} - Q^p.$$

Here, $\phi = 0.5$ and p denote the subiteration number. The deduced subiteration scheme reverts to the standard LU-SGS scheme as $\phi = 0$ and $p = 1$. In fact, regardless of the temporal accuracy of the left hand of equation (9), second-order time accuracy is maintained when the subiteration number tends to infinity.

In the multiblock-grid method, the Navier–Stokes equations are solved in each block separately. The calculation of convective and viscous fluxes at block boundaries needs flowfield values of two grid points in abutting blocks, so the lagged flowfield always exists due to the lagged block boundary condition. Rizzetta and Visbal (1993) considered that the subiteration can eliminate errors from linearization, factorization, lagged boundary conditions and lagged turbulence models.

For the unsteady flutter calculation, at each real time step, through subiteration between fluid and structural

equations (6) and (9), the time accuracy of the whole computation has second order. Therefore, the subiteration method is very important not only for eliminating the lagged flowfield induced by lagged multiblock boundary condition but also for removing the sequencing effects between the fluid and structure. In addition, in practical application, the number of subiterations is commonly taken as a fixed value. Since the restricted number of iterations does not remove sequencing effects and factorization errors at every time step completely, a proper time-step size needs to be evaluated by numerical tests. Similarly, the fixed time-step size is used for these calculations.

4. Multiblock moving grid deformation

For a complex aerodynamic configuration, the multi-block grid-generation is a major challenge. Grid topology may be further limited due to the technique of moving grid deformation. In the paper, one of the aircraft configurations calculated is shown in figure 1. The surface grid is first distributed, which contains 5 zones, 3 zones for fuselage and 2 zones for the main wing and the horizontal wing, respectively. A total of 10 zones are distributed on the whole surface. An H-type multiblock grid with 40 blocks is depicted. To save computational time and allow the grid deformation more easily, multiblock grid generated guarantees block boundaries in the k direction located in the surface of the wall and far field. Then the grid deformation on the far grid boundary can be set to be zero and the deformations on the wall surface are obtained using the structural equation of motion. The deformation values in the inner grid are interpolated with the TFI method. The deformations are added to the original grid to obtain the new adaptive multiblock grid. For the small and moderate aeroelastic deformation, this method maintains the grid quality of the original grid and maximizes the re-usability of the original grid.
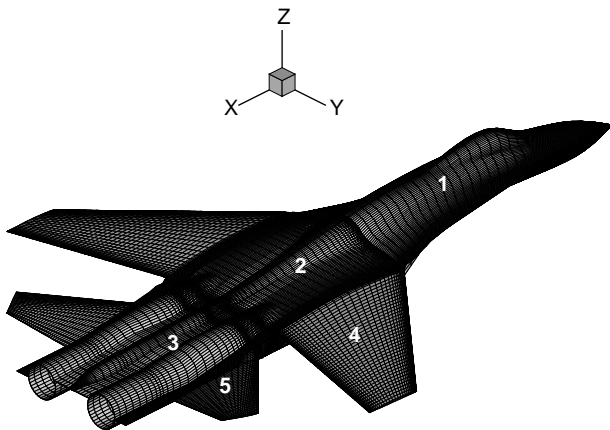

Figure 1.   Surface grid.

5. Data transformation

For these aeroelastic calculations, the structural model data are provided using a plate model and only normal deformation is considered. However, the real geometry is used for the fluid solution. Then the problem of passing information between the fluid and structural grids becomes very complicated. The fluid grid is first projected to the surface of the structural grid and the deformations on the projected fluid grid points are interpolated by the infinite plate spline (IPS) and the principal of virtual work, which can guarantee the conservation of energy between the fluid and structural systems.

6. Results and discussions

6.1 Standard aeroelastic wing

Aeroelastic wind-tunnel experiments are intrinsically destructive and hence much more expensive than a similar rigid-body experiment. Suitable experimental data to validate the aeroelastic solver is scarce. A complete aeroelastic experiment is available for the AGARD 445.6 standard aeroelastic wing, which has been used to validate flutter simulations in most publications. The disadvantage of this case is that the nonlinear character is relatively weak due to a thin wing, in the absence of a better experiment data, the experiment is used to evaluate the current method.

The AGARD 445.6 wing model has an aspect ratio 1.6525, a taper ratio of 0.6576, a quarter-chord swept angle of 45 deg and a NACA 65A004 airfoil section. The first four structural modes and natural frequencies provided in Yates (1988) are used directly for these computations. The number of total grid cells is about 744.000, which distributes 81×39 grid lines on the lower and upper surfaces, respectively, and 63 grid lines in the normal direction. Structural damping coefficient is set as zero and the time-step size is taken as 0.01. Each Mach number is run for several dynamic pressures to determine the flutter point. The flutter boundary and frequency over the Mach number range of 0.338–1.141 are calculated and compared with experimental data in figure 2. The typical transonic dip phenomenon is well captured. In the subsonic and transonic range, the calculated flutter speeds and frequencies agree well with experimental data, however, in the supersonic range, the present calculation overpredicts the experimental flutter points similar to other computations.

6.2 A tail wing with control surface

The structural model contains the main tail wing and the tail control surface, which distribute 3 zones which contain 51×37, 71×20, 21×30 grid lines on each zone. Flutter characters of the configuration with two structural modes for the design points of Mach number 0.6
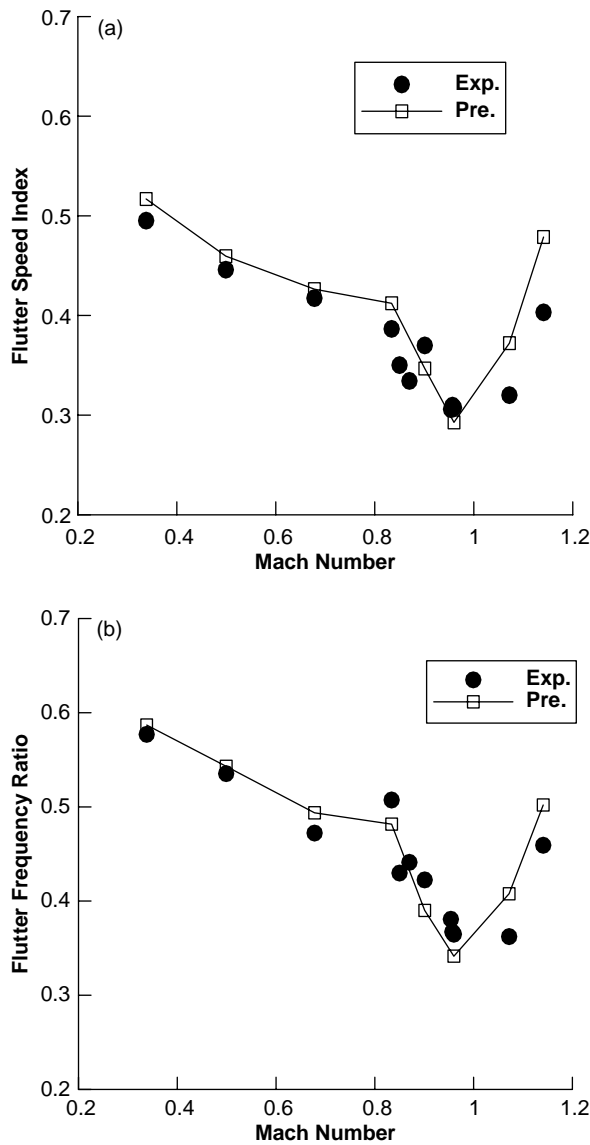
Figure 2. (a) Flutter speed and (b) flutter frequency for the AGARD standard aeroelastic wing.

and 0.95 are analyzed. The first 10 structural mode shapes and frequencies for the 0.95 design point are shown in figure 3(a–j). The varying density method is used to determine the flutter boundary, the time histories of generalized displacements with different density can be calculated. Based on the divergence and convergence of the time responses of the generalized displacement, the flutter dynamic pressure and frequencies are determined. Figure 4(a–d) only shows several typical results at Mach numbers of 0.8, 0.95, 0.98 and 1.3. For example, at Mach number of 0.95, the time history tends to convergence at varying density coefficient of $c = 0.89$ and divergence at $c = 0.90$. After Mach number of 1.3, the time history of the first mode is still converging but its third mode divergences. At this time, the flutter boundary should be determined based on the time history of generalized displacement of the third mode. Flutter dynamic pressure and frequencies for the two tail wing structural models at

the design points of Mach numbers of 0.95 and 0.6 are shown in figure 5. Transonic flutter dip is found at the Mach number of 1.02, comparing the Mach number of 0.9, the dynamic pressure and frequency at flutter dip decrease 40 and 20% for the structural model of the design point $M = 0.95$ and 35% and 16% for the structural model of the design point $M = 0.6$, respectively.

6.3 A complex aircraft model

The final calculation is taken for the configuration of figure 1. The first seven modes are considered. For this case, flutter is analyzed with the varying structural stiffness, namely, the freestream density and temperature are assumed unchanged sea level values, then dynamic pressure can be calculated for a different Mach number. Under the fixed Mach number and dynamic pressure, a stiffness coefficient of f_i is introduced into the structural equation of motion of equation (3). Equation (3) becomes

$$\ddot{q}_i(t) + 2\zeta_i\omega_i\dot{q}_i(t) + \left(f_i\omega_i\right)^2 q_i(t)$$

$$= \frac{q_\infty \oint_S \int [\Phi]_i^T \Delta C p_i \, dS}{M_i}. \tag{10}$$

Such as for $f_i = 0.7$, it is indicated that the structural stiffness calculated is only 70% of the original stiffness. For different stiffness coefficient, the dynamic responses may be convergent or divergent and if the value of stiffness coefficient at the flutter boundary is interpolated, then flutter dynamic pressure and frequency for the original aircraft can be calculated with $q_f = q_\infty/f$ and $\omega_f = \omega/\sqrt{f}$. Figure 6 shows the flutter boundaries of dynamic pressure and frequency vs. the Mach numbers. In the figure, the real line represents the results of this calculation and the dash line is the result of Lu *et al.* (2003). The frequencies are in good agreement with each other except at supersonic Mach numbers of 1.1 and 1.3. The error of dynamic pressure is about 12%. The results show, for the aircraft, there is no obvious transonic dip for dynamic pressure in the whole Mach number ranges and only a small decrease in frequency at the around Mach number of 0.9.

7. Conclusions

A fully implicit aeroelastic solver has been developed for fluid/structure interaction on complex configuration through the tightly coupled solution of the Navier–Stokes equations and the structural equations of motion. Navier–Stokes equations are discretized with a LU-SGS subiteration algorithm and the HLLEW scheme. Structural equations of motion are discretized directly by a second scheme with subiteration in generalized coordinates. Multiblock grid deformation is performed with the TFI method. IPS and the principle of virtual work are used for data transformation of deformation and force between

f_m1 = 16.59Hz

Structural Model (M_∞ = 0.95)
(a) The first mode

f_m2 = 24.44Hz

Structural Model (M_∞ = 0.95)
(b) The second mode

f_m3 = 52.90Hz

Structural Model (M_∞ = 0.95)
(c) The third mode

f_m4 = 55.58Hz

Structural Model (M_∞ = 0.95)
(d) The fourth mode

f_m6 = 105.40Hz

Structural Model (M_∞ = 0.95)
(e) The fifth mode

f_m6 = 105.40Hz

Structural Model (M_∞ = 0.95)
(f) The sixth mode

f_m7 = 108.02Hz

Structural Model (M_∞ = 0.95)
(g) The seventh mode

f_m7 = 108.02Hz

Structural Model (M_∞ = 0.95)
(h) The eighth mode

f_m9 = 118.75Hz

Structural Model (M_∞ = 0.95)
(i) The ninth mode

f_m10 = 123.54Hz

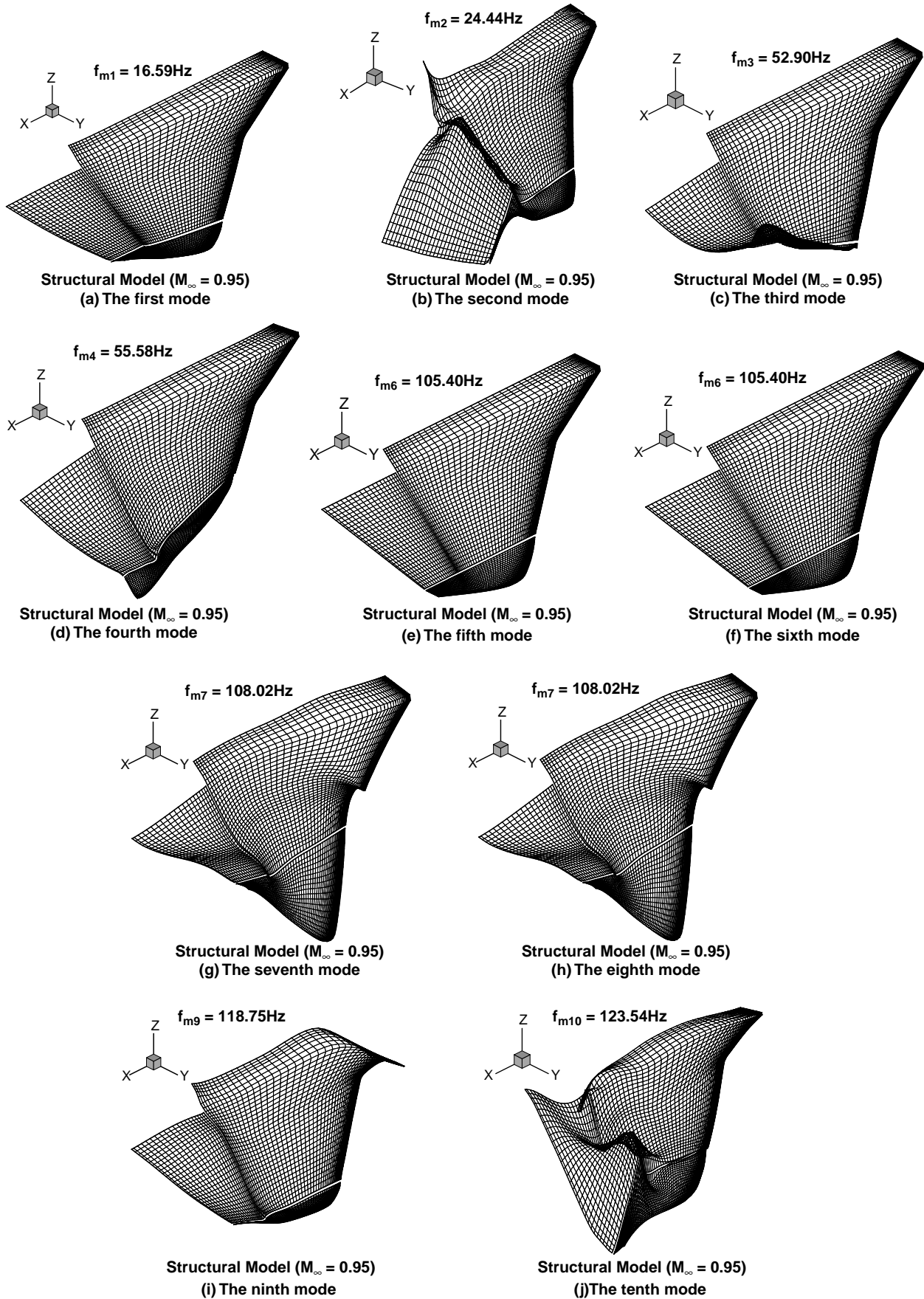**Structural Model (M_∞ = 0.95)**
(j)The tenth mode

Figure 3. First 10 modes and natural frequencies for the structural model of $M = 0.9$. (a) The first mode, (b) the second mode, (c) the third mode, (d) the fourth mode, (e) the fifth mode, (f) the sixth mode, (g) the seventh mode, (h) the eighth mode, (i) the ninth mode, and (j) the tenth mode.
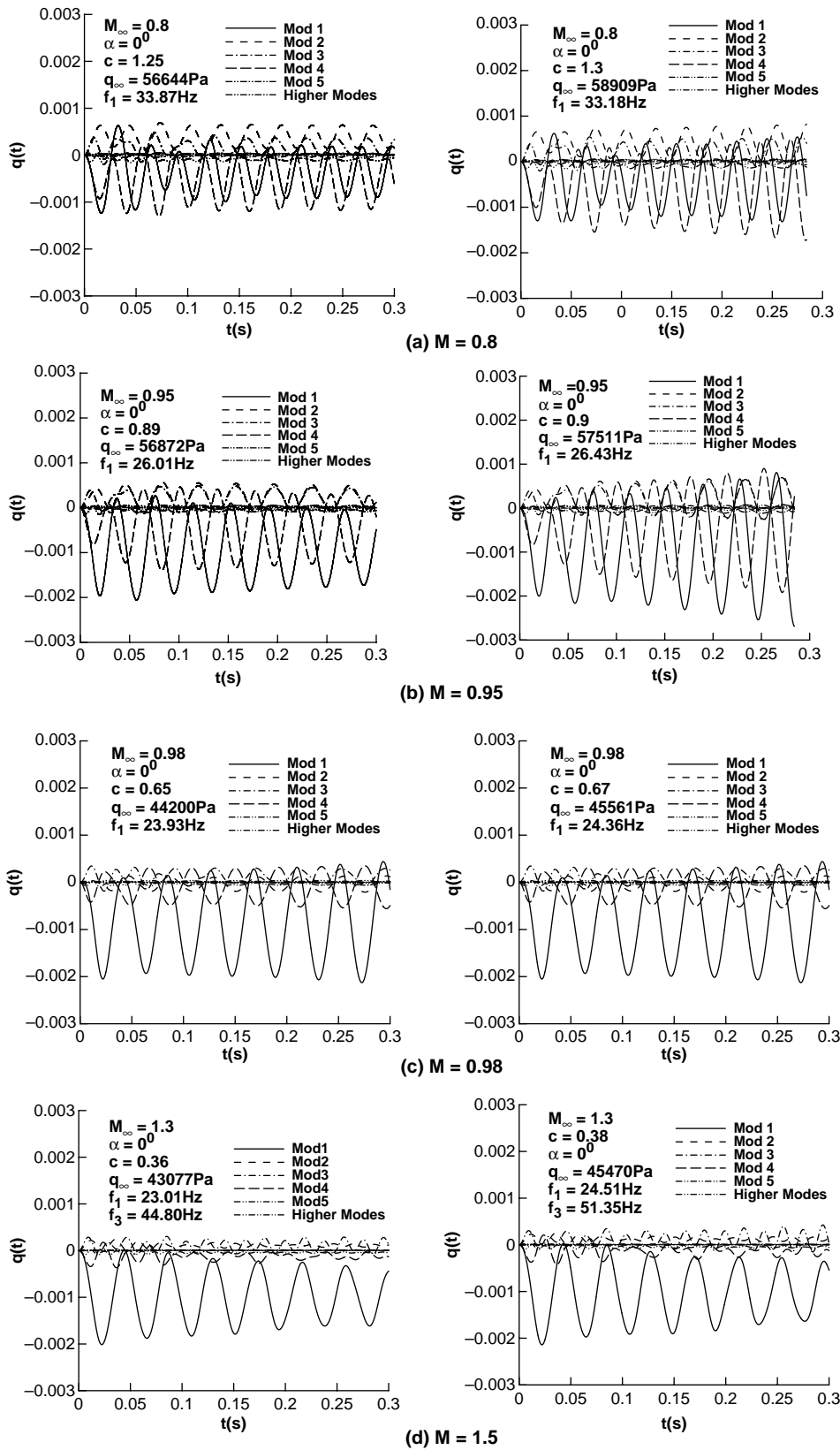
Figure 4.   Time histories of the generalized displacement for the design model of $M = 0.95$. (a) $M = 0.8$, (b) $M = 0.95$, (c) $M = 0.98$, (d) $M = 1.5$.

the fluids and the structures. The experiment of the AGARD 445.6 standard aeroelastic wing was used to validate the code. For the tail wing with the control surface, the flutter boundaries on two structural models at

design points of Mach number 0.95 and 0.6 were calculated. For this case, when the Mach number is larger than 1.3, the time histories of the third modes would diverge first. Finally, a complex aircraft configuration has
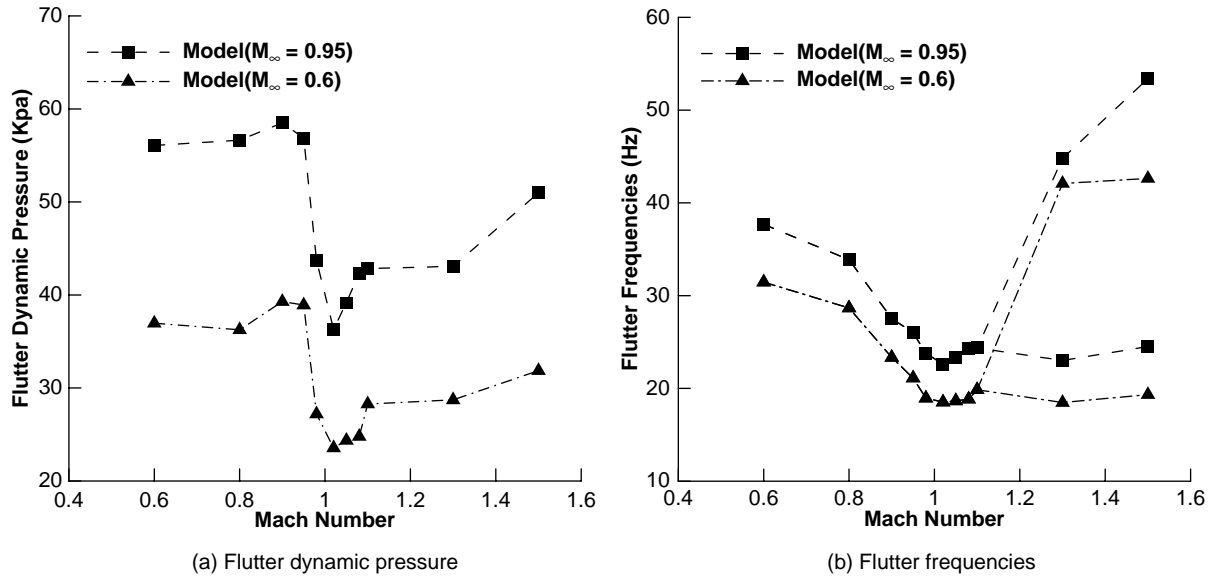
(a) Flutter dynamic pressure　　　　　　　　　(b) Flutter frequencies

Figure 5.　Flutter dynamic and frequencies for the design models of $M = 0.95$ and 0.6. (a) Flutter dynamic pressure and (b) flutter frequencies.
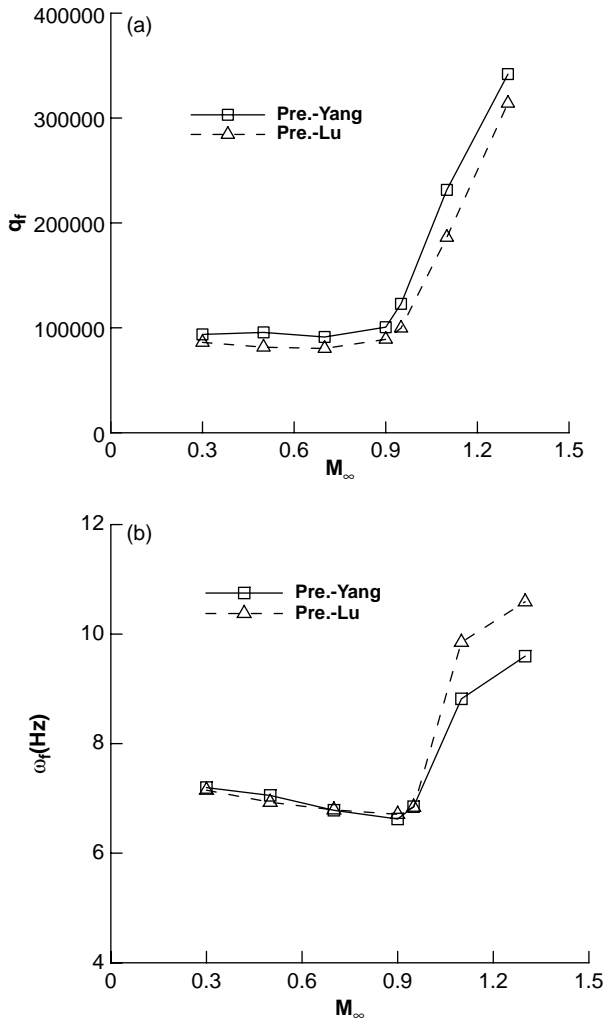

Figure 6.　(a) Flutter dynamic pressure and (b) flutter frequency.

been simulated with the solver. There is no obvious transonic dip in the whole Mach number range. Through the above three calculations, we can find, for different configurations, the position of the transonic dip locates in the different range of Mach number. All of the results indicate the developed code can treat the problems of complex unsteady fluid/structure interaction.

References

Alonso, J.J. and Jameson, A., Fully-implicit time-marching aeroelastic solutions. *AIAA Paper*, 94-0056, 1994.

Anderson, W.K., Thomas, J.L. and van Leer, B., A comparison of finite volume flux vector splittings for the Euler equations. *AIAA Paper*, 85-0122, January, 1985.

Appa, K., Finite-surface spline. *Journal of Aircraft*, 1989, **26**, 495–496.

Einfeldt, B., Munz, C.D., Roe, P.L. and Sjoegree, B., On Godunov-type methods near low densities. *Journal of Computational Physics*, 1991, **92**, 273–295.

Gordnier, R.E. and Melville, R.B., Transonic flutter simulations using an implicit aeroelastic solver. *Journal of Aircraft*, 2000, **37**, 872–879.

Goura, G.S.L., Badcock, K.J., Woodgate, M.A. and Richards, B.E., Implicit method for the time marching analysis of flutter. *The Aeronautical Journal*, 2001a, **105**, 199–214.

Goura, G.S.L., Badcock, K.J., Woodgate, M.A. and Richards, B.E., A data exchange method for fluid–structure interaction problems. *The Aeronautical Journal*, 2001b, **105**, 215–221.

Guruswamy, G.P., Vortical flow computations on swept flexible wings using Navier–Stokes equations. *AIAA Journal*, 1990, **28**, 2077–2084.

Harder, R.L. and Desmarais, R.N., Interpolation using surface splines. *Journal of Aircraft*, 1972, **9**, 189–191.

Lee-Rausch, E.M. and Batina, J.T., Wing flutter computations using an aeroelastic model based on the Navier–Stokes. *Journal of Aircraft*, 1996, **33**, 1139–1147.

Liu, F., Cai, J., Zhu, Y., Tsai, H.M. and Wong, A.S.F., Calculation of wing flutter by a coupled fluid–structure method. *Journal of Aircraft*, 2001, **38**(2), 334–342.

Lu, Z.L., Guo, T.Q. and Guan, D., Numerical algorithm on compressible flutter. *Proceeding of the Symposium of the Eighth Chinese Aeroelasticty*, An'Shan, Aug. 2003, pp. 14–24.

Melville, R.B., Morton, S.A. and Rizzetta, D.P., Implementation of a fully-implicit, aeroelastic Navier–Stokes solver. *AIAA Paper*, 97-2039, 1997.

Potsdam, M.A. and Guruswamy, G.P., A parallel multiblock mesh movement scheme for complex aeroelastic applications. *AIAA Paper*, 01-0716, 2001.

Rizzetta, D.P. and Visbal, M.R., Comparative numerical study of two turbulence models for airfoil static and dynamic stall. *AIAA Journal*, 1993, **31**, 879–889.

Thomas, P.D. and Lombard, C.K., Geometric conservation law and its application to flow computations on moving grid. *AIAA Journal*, 1979, **17**(10), 1030–1037.

Wong, S.F., Tsai, H.M., Cai, J., Zhu, Y. and Liu, F., Unsteady flow calculations with a multi-block moving mesh algorithm. *AIAA Paper*, 00-1002, 2000.

Yang, G., Obayashi, S., Nakamichi, J. and Buzz, A., Simulation using an implicit multibolk aeroelastic solver. *Journal of Aircraft*, 2003, **40**(3), 580–589.

Yates, E.C. Jr., AGARD standard aeroelastic configurations for dynamic response I-wing 445.6, ARARD-R-765, July, 1988.

Yoon, S. and Jameson, A., Lower–upper symmetric-Gauss–Seidel method for the Euler and Navier–Stokes equations. *AIAA Journal*, 1988, **26**, 1025–1026.